Desalination and Water Treatment
www.deswater.com

doi:10.5004/dwt.2017.20332

68 (2017) 274–292
March

Removal of Congo red dye from aqueous solutions by adsorption onto a dual adsorbent (*Neurospora crassa* dead biomass and wheat bran): optimization, isotherm, and kinetics studies

P. Vairavel[a,*], V. Ramachandra Murty[b], S. Nethaji[a]

[a]*Department of Chemical Engineering, Manipal Institute of Technology, Manipal University, Manipal, India, Tel. +91 9036270978, email: pvairavel@gmail.com (P. Vairavel), Tel. + 91 8123244744, email: nethajis6587@yahoo.com (S. Nethaji)*
[b]*Department of Biotechnology, Manipal Institute of Technology, Manipal University, India, Tel. +91 9448529691, email: murty.vytla@manipal.edu*

Received 3 May 2016; Accepted 6 November 2016

ABSTRACT

In this study, the dead biomass of *Neurospora crassa* along with wheat bran was used as a dual adsorbent for the removal of congo red from aqueous solutions. Decolorization experiments were conducted in batch mode by varying experimental factors such as initial pH, adsorbate concentration, wheat bran dosage, and dead biomass dosage. The experiments were designed to attain the most optimized system. The zero-point charge of the dual adsorbent was 9. The experimental equilibrium data for the decolorization of congo red were evaluated by various isotherm models. Kinetic rate constants were found using different kinetic models. The adsorption mechanisms were described by pore diffusion and Boyd plots. The dye adsorption rate followed pseudo-second-order kinetic model, and the equilibrium data were appropriately fitted to Langmuir adsorption isotherm. The overall rate of adsorption is controlled by both film diffusion and pore diffusion of dye molecules. Thermodynamic studies were performed to determine the change in Gibbs free energy (ΔG), change in enthalpy (ΔH), and change in entropy (ΔS) of the adsorption process. The adsorption was found to be endothermic in nature, and the process was spontaneous and favorable. Desorption studies were conducted using various desorbing agents. The maximum percentage of dye was desorbed using the solvent methanol.

Keywords: Congo red dye; *Neurospora crassa* dead biomass; Wheat bran; Equilibrium; Kinetics; Isotherms

1. Introduction

The effluents discharged from several industries,such as paper, textile, cosmetic, food, printing, pharmaceutical, and plastics industries, contain highly colored synthetic dyestuff. This dyestuff is released into the environment and is a major cause of environmental pollution [1]. The major contaminants in dye-house effluents are unfixed dyes on fibers, auxiliary dyeing chemicals, salts, acids, bases, and chlorinated compounds [2]. It is known that 5–15% of untreated dyes are discharged in dyeing processes [3]. Generally, color is visible in the effluents from textile-dyeing processes when the dye concentration is greater than 1 mg/L and at an average concentration of 300 mg/L [4]. Approximately 1×10^5 dyes are presently in commercial use. The annual worldwide production of dyes is 7×10^5 tons [3]. Among these, the synthetic dye congo red (CR) is a popular water-soluble, acidic, anionic dye. It shows a high affinity for cellulose fibers and is used in the textile processing industry [1]. This dye is known to be metabolized to

*Corresponding author.

benzidine, which is a human carcinogen [5]. With increasingly stringent discharge standards, it has become necessary to develop technological systems for minimizing the concentration of dyes in wastewater. The removal of such colored substances from industrial wastewater has great environmental and commercial importance.

Most dye effluents can be treated by several methods, including coagulation, membrane filtration, adsorption, advanced oxidation processes, biodegradation, and biosorption [6,7]. Many of these methods, excluding adsorption, suffer from the drawbacks of capital as well as high operational costs and the need to dispose sludge formed in the process [6,8]. Adsorption is superior for water recycling in terms of its simplicity and ease of operation [1,6]. Activated carbon is the preferred adsorbent in many industries and is used to remove various dyes from effluents. However, its wide use is limited by its higher cost. To reduce the cost of the treatment process, researchers have made good use of many cheaper and effective adsorbents from natural sources [6]. These include agricultural waste materials, such as wheat bran [9], lotus leaf [10], peat [11], neem leaf powder [12], rice husk [13], wheat straw [14], etc., which have been used for removing color from dye wastewater. In biological treatments, live biomass is used to biodegrade and biosorb dye molecules, whereas dead biomass is used only to adsorb dye molecules. Various types of dead fungal biomass can be used to decolorize dye wastewater, such as *Phanerochaete chrysosporium* [15], *Aspergillus niger* [16], *Rhizopus arrhizus* [17], *Trametes versicolor* [18], *Funalia trogii* [19], and *Neurospora crassa* [20], among others. The removal of color from dye wastewater using dual adsorbent remains a relatively unexplored area. The literature survey indicates that decolorization studies of organics in this area are limited. Biosorption of selected toxic organics with few types of bacterial or fungal biomass and the use of agricultural waste as a low-cost adsorbent of dye molecules have been investigated. Therefore, the present study was performed to investigate the use of dead fungal biomass of *Neurospora crassa* with wheat bran as a dual adsorbent for the decolorization of CR dye from synthetic dye wastewater. *Neurospora crassa* is a filamentous ascomycete nonpathogenic fungus. Wheat bran is the outer cover of the wheat kernel and a by-product of the wheat milling operation; furthermore, it is the most readily available natural material in India.

2. Materials and methods

2.1. Preparation and characterization of wheat bran and dead biomass biosorbent

Wheat bran was procured from a wheat grinding mill and was washed with distilled water to remove impurities. Then, it was dried in a hot-air oven at the temperature of 105°C for 24 h, ground, and screened to obtain particles < 100 µm in size. The filamentous fungus *Neurospora crassa* (MTCC 1852) used in this study was obtained from the Institute of Microbial Technology, Chandigarh, India, and was stored at 4°C. In total, 100 mL of potato dextrose broth media was inoculated with the live fungal culture under sterile conditions in Erlenmeyer flasks. The fungi were permitted to grow for a week in an incubator shaker rotated at a speed of 120 rpm at 25°C. After sufficient growth, the live fungal biomass was filtered and washed thoroughly with distilled water. It was then oven-dried overnight on petri plates at 60°C and powdered using a mortar and pestle. The material was screened to obtain particles < 100 µm in size. The dual adsorbent was characterized by particle size, zero-point charge, Fourier Transform Infrared Spectroscopy (FT-IR), Scanning Electron Microscopy (SEM), surface area, and porosity. The pH point of zero-point charge (pH_{zpc}) of the dual adsorbent was found by the solid addition technique [21].

2.2. Preparation of CR dye stock solution

Analytical grade CR dye was obtained from Sigma-Aldrich, India. The required amount of dye powder was dissolved in distilled water to prepare a 1000 mg L^{-1} stock solution. This stock solution was further diluted with distilled water to obtain the required concentration range.

2.3. Analytical measurements

A double-beam UV/visible spectrophotometer (Shimadzu UV-1800) operating at the wavelength (λ_{max}) of 498 nm was used to determine the unknown residual concentration of the CR dye solution. The pH of the dye solution was observed by a digital pH-meter (Systronics 335), and the average particle size of the dual adsorbent was evaluated by a particle size analyzer (Cilas 1064, France). The surface area and pore volume of the dual adsorbent were determined using a Brunauer–Emmett–Teller (BET) surface analyzer (Smart Instruments, India). FT-IR (Shimadzu 8400S, Japan) was used to determine the functional groups in the dual adsorbent before and after adsorption. The surface morphology of dual adsorbent before and after adsorption was analyzed by SEM(JEOL JSM 6380LA, Japan).

2.4. Adsorption experiments

The factors influencing the decolorization of dye wastewater, such as the initial pH, adsorbate concentration, wheat bran dosage, and dead biomass dosage, were optimized in batch studies. Adsorption equilibrium experiments were conducted using a fixed dual adsorbent dosage by changing the initial adsorbate concentration from 100 to 400 mg L^{-1} and stirring the solutions at 200 rpm for 24 h at 303 K. The adsorption kinetics experiments were performed at various adsorbate concentrations (50 mg L^{-1} to 300 mg L^{-1}) with a fixed dual adsorbent dosage and at constant temperature. A known amount of solution was withdrawn at regular intervals. The amount of CR dye adsorbed onto a unit mass of dual adsorbent at equilibrium and the percentage decolorization [10,22] were determined using Eqns. (1) and (2), respectively.

$$q_e = \frac{(C_o - C_e)v}{w} \tag{1}$$

$$\%\,\text{removal} = \frac{(C_o - C_e)\times 100}{C_o} \tag{2}$$

where C_o and C_e are the initial and equilibrium adsorbate concentrations in solution (mg L^{-1}), V is the dye solution volume (L), and W is the weight of the dry dual adsorbent (g).

2.5. Factorial experimental design

Factorial experimental design was used to obtain the overall best optimization and to minimize the number of experimental trials. Influencing factors, such as pH (X_1), initial adsorbate concentration (X_2), wheat bran dosage (X_3), and dead biomass dosage (X_4) were kept as independent variables while the percentage decolorization was set as the response variable. The experiments were conducted in 31 trials (16 cube point, 7 center point, and 8 axial point), based on a central composite design (CCD) matrix using 2^4 full factorial design. The levels of independent variables were coded as –α (very low), –1 (low), 0 (central point), 1 (high), and α (very high). The performance of the system was described by a second-order polynomial equation [23,24]:

$$Y = \beta_o + \sum \beta_i x_i + \sum \beta_{ii} x_i^2 + \sum \beta_{ij} x_i \quad (3)$$

$$x_i = \frac{x_i - x_o}{\delta x} \quad (4)$$

where Y is the predicted response variable of percentage decolorization; β_o is the offset term; x_i is the coded experimental level of the variable X_i; X_o is the center point value of X_i; δX denotes the step change; and β_i, β_{ii}, and β_{ij} are the regression coefficients for linear, squared, and interaction effects, respectively. The Minitab 16 statistical software was used to study and explain the results of the experimental design to find the response variable.

2.6. Desorption studies and reusability of the dual adsorbent

Desorption studies were performed by using various desorbing agents, such as ethanol, methanol, iso-propyl alcohol, 1 M NaOH, acetone, water, 1 M $CaCl_2$, 1 M NH_4OH, 1 M Na_2CO_3, 1 M $NaHCO_3$, and 0.1 M NaOH [25,26]. In a typical desorption experiment, the above mentioned desorbing agents were added to the dual adsorbent with adsorbed dye and agitated for a sufficient duration in separate batches. The process was continued till the dye was desorbed by the desorbing agent, following which the centrifugation process was used to separate the regenerated dual adsorbent and desorbed dye molecules. The desorption for the second and third runs was carried out with 100 mL of the above-mentioned variety of reagents in separate batches. The dual adsorbent after desorption was collected by centrifugation and was left to dry at 60°C for 24 h. The percentage color removal by the regenerated dual adsorbent was tested (2nd and 3rd run) under the optimized values of the process factors and compared with the first use.

3. Results and discussion

3.1. Characterization of the dual adsorbent

The surface area and pore volume of the dual adsorbent were obtained from adsorption of nitrogen at 77 K. The BET surface area of the dual adsorbent was 2.4 $m^2 g^{-1}$. The pore volume was found to be 1.8 $mm^3 g^{-1}$, with the average particle size of 49.60 µm. The physical characteristics of the dual adsorbent were determined, and the results are reported in Table 1. FTIR spectra of the dual adsorbent before and after CR dye adsorption are shown in Fig. 1. The FTIR spectrum of the dual adsorbent before adsorption shows a broad and strong peak at 3531 cm^{-1}, representing the O–H stretching of bonded hydroxyl groups on the surface of the dual adsorbent. The narrow and strong peak at 2927 cm^{-1} was attributed to the C–H bending vibrations of methyl ($–CH_3$) and methylene groups. The peak observed at 2360 cm^{-1} was due to O=C=O stretching. The bending vibrations of –OH and stretching vibrations of C–O–C were observed in the form of the peak at 1022 cm^{-1}. Similarly, the presence of C=O stretching vibrations of carbonyl groups of aldehyde and ketones was observed from the peak at 1654 cm^{-1}. The C–H bending vibrations of the CH_2 group were identified by the peak at 1469 cm^{-1}. After adsorption, it was observed that the peaks of the O–H stretching vibrations of the hydroxyl groups, C–H bonds of methyl groups, and C=O bonds of carbonyl groups were shifted from 3531 cm^{-1}, 2927 cm^{-1}, and 1654 cm^{-1} to 3614 cm^{-1}, 2923 cm^{-1}, and 1632 cm^{-1}, respec-

Table 1
Physical properties of dual adsorbent

Parameters	Values
Moisture content (%)	4.68
Volatile matter (%)	51.47
Ash content (%)	7.81
Fixed carbon (%)	36.04

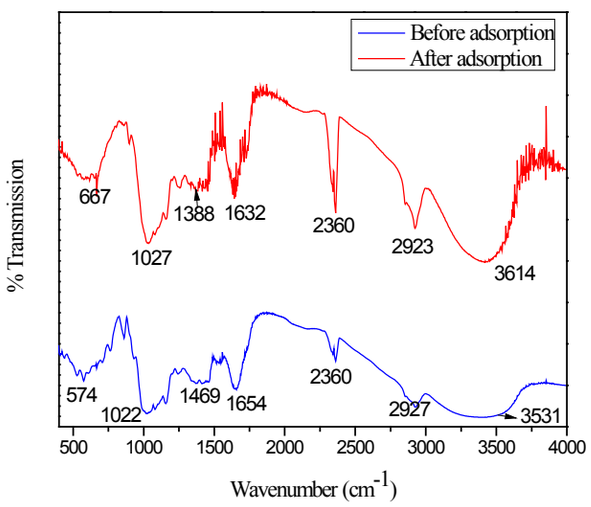

Fig. 1. FTIR spectrum of dual adsorbent before and after congo red dye adsorption.

tively. Thus, the FTIR analysis demonstrated that more hydroxyl, methyl, and carbonyl groups were present on the surface of the dual adsorbent. These groups may act as possible binding sites for electrostatic interactions with the anionic dye molecules. SEM micrographs of the dual adsorbent before and after adsorption of CR dye were shown in Fig. 2a and 2b respectively. The dual adsorbent had rough fibrous morphology as seen in Fig. 2a. The presence of CR dye molecules onto the surface of the dual adsorbent after adsorption was evident from Fig. 2b.

3.2. Batch adsorption studies

Adsorption of the CR dye by the dual adsorbent is affected by the pH of the dye solution and the zero-point charge of the dual adsorbent. The plot of ΔpH vs. initial pH is shown in Fig. 3. The zero-point charge is the initial pH when the curve crosses zero on the ΔpH scale. The zero-point charge (pH_{zpc}) on the surface of the dual adsorbent has been found to occur at pH 9. The presence of H^+ and OH^- ions in solution may change the potential surface charges of the dual adsorbent. If the pH of the solution is below the zero-point charge, the active sites on the surface of the dual adsorbent will be protonated by the presence of excess H^+ ions. If it is above its zero-point charge, the active sites on the surface will be deprotonated by the OH^- ions present in the solution. Batch adsorption studies were conducted by fixing one factor at a time and by varying the other factors simultaneously. It was difficult to analyze the effect of the initial pH on dye decolorization under a strongly acidic pH because of the formation of protonated species, which may lead to a change in the structure of the dye. The CR dye in aqueous solution was black in color at acidic pH (< 5), due to the formation of a quinonoid structure [27]. The red color remained stable in the pH range of 6–12. Therefore, the influence of the initial pH on color removal was analyzed between pH 6–12. The decolorization of the CR dye was found to decrease from 93.80 to 53.24% with increasing pH (Fig. 4). This phenom-

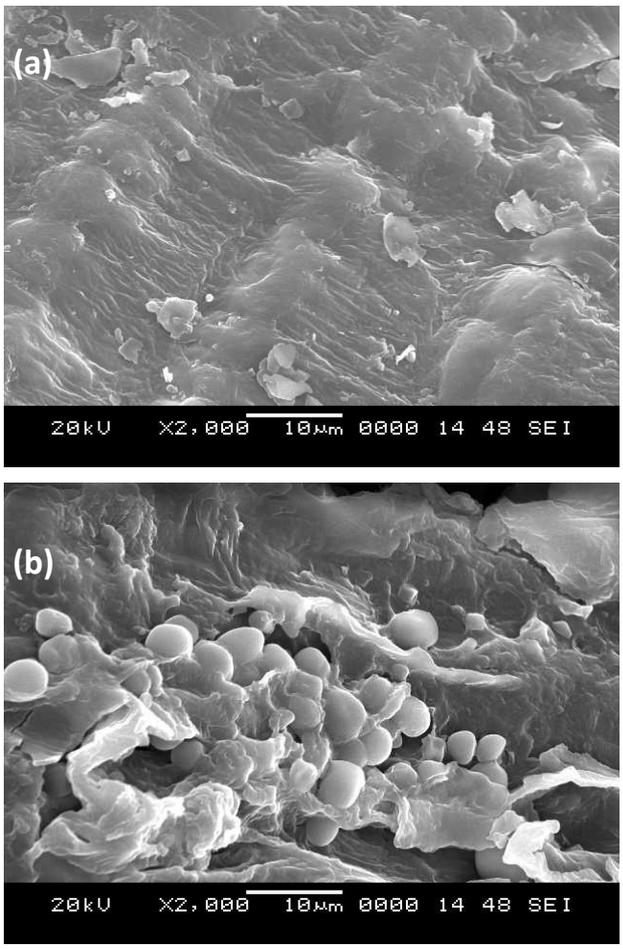

Fig. 2. SEM micrograph of (a) dual adsorbent before CR dye adsorption (b) dual adsorbent after CR dye adsorption.

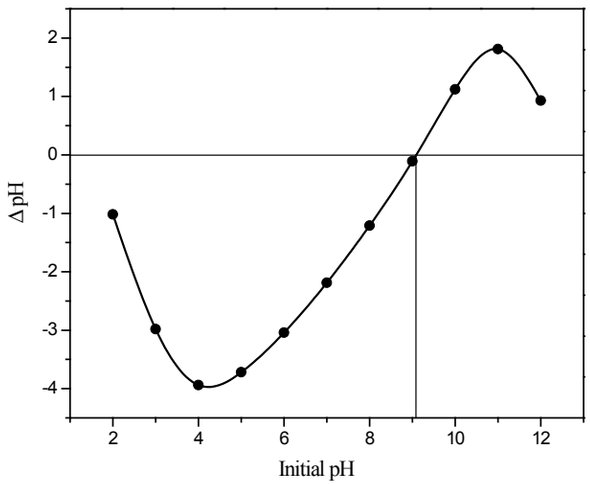

Fig. 3. Zero point charge plot of dual adsorbent.

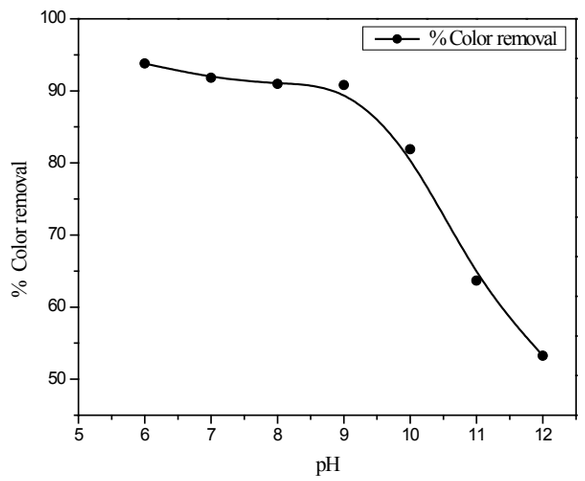

Fig. 4. Effect of initial pH on removal of CR dye by dual adsorbent. (Adsorbate concentration: 200 mg L^{-1}; wheat bran dosage: 12.5 g L^{-1}; dead biomass dosage: 2 g L^{-1}; agitation speed: 200 rpm; Temperature: 303 K; contact time 10 h).

enon could be due to the increase in the repulsive forces between the functional groups present on the surface of the dual adsorbent and the CR dye molecules. The lower percentage adsorption of CR observed at basic pH is also due to competition between the excess hydroxyl ions and the negatively charged dye ions for the adsorption active sites [20]. In the pH range from 6 to 9, the dye molecules exhibited greater affinity to the positively charged binding sites of the dual adsorbent. The influence of the adsorbate concentration was analyzed by changing the initial adsorbate concentration from 100 to 500 mg L^{-1}. The increase in dye concentration reduced the decolorization of the CR dye from 98.80 to 84.31% (Fig. 5) because of the accumulation of adsorbate in the vacant sites (lack of available active sites) and the competition between more dye molecules at the fixed binding sites of the dual adsorbent [28,29]. As the initial adsorbate concentration was increased, the available binding sites on the surface of the dual adsorbent were saturated, leading to the decrease of the percentage decolorization. The effect of wheat bran dosage on color removal was analyzed by varying the wheat bran dosage per 100 mL of dye solution. The amount of dye adsorbed on the dual adsorbent at equilibrium q_e (mg g^{-1})decreased from 35.78 to 13.35 mg g^{-1}, but the decolorization efficiency increased from 83.49 to 97.88% with the increase in wheat bran dosage from 0.5 to 2.0 g (Fig. 6). Similarly, the effect of dead biomass dosage was analyzed by varying the dosage from 0.05 to 0.5 g. The increase in dead biomass dosage increased the color removal percentage from 76.45 to 95.42% (Fig. 7). This is because, the increase in the adsorbent dosage resulted in the increase in the amount of active surface sites available for the adsorption of CR dye. However, when the adsorption capacity is expressed in mg dye adsorbed per gram of the adsorbent (q_e), the capacity decreased from 21.84 to 19.08 mg g^{-1} with the increase in the dead biomass dosage(Fig. 7).This is due to the split in the flux or concentration gradient between the adsorbate concentration in the solution and that at the surface of the dual adsorbent. Thus the competition for the availability of active sites for the adsorption of dye decreases with the increase in the adsorbent dosage. In other words, at higher adsorbent (wheat bran/dead biomass)-to-solute concentration ratios, adsorption onto the dual adsorbent surface is very rapid, thus producing a lower solute concentration in the solution, compared to that obtained for a lower dual adsorbent-to-solute concentration ratio [29]. Hence, the amount of CR dye adsorbed onto a unit weight of dual adsorbent (q_e) gets decreased with increase in adsorbent dosage.

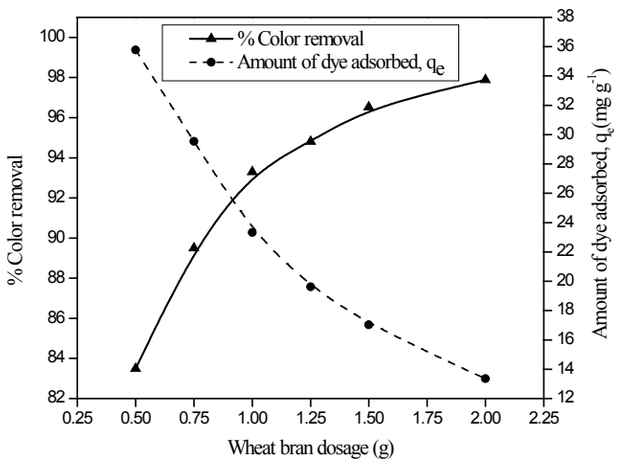

Fig. 6. Effect of wheat bran dosage on removal of CR dye by dual adsorbent.
(pH: 6; adsorbate concentration: 300 mg L^{-1}; dead biomass dosage: 2 g L^{-1}; agitation speed: 200 rpm; Temperature: 303 K; contact time 24 h).

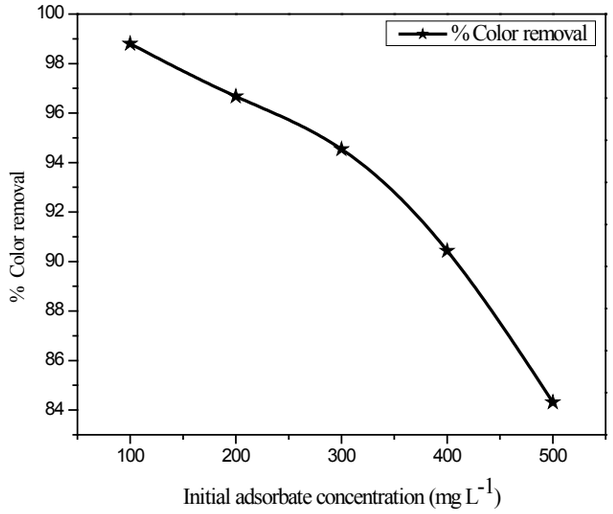

Fig. 5. Effect of initial adsorbate concentration on removal of CR dye by dual adsorbent.
(pH: 6; wheat bran dosage: 12.5 g L^{-1}; dead biomass dosage: 2 g L^{-1}; agitation speed: 200 rpm; Temperature: 303 K; contact time: 10 h).

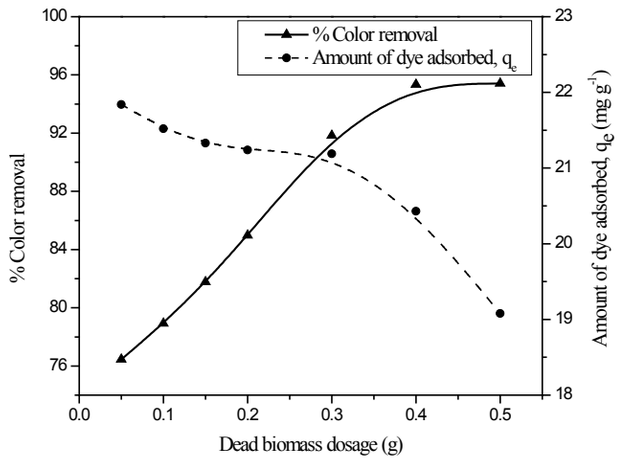

Fig. 7. Effect of dead biomass dosage on removal of CR dye by dual adsorbent.
(pH: 6; adsorbate concentration: 300 mg L^{-1}; wheat bran dosage: 10 g L^{-1}; agitation speed: 200 rpm; Temperature: 303 K; contact time 24 h).

3.3. Factorial experimental design and parameter optimization

Various groups of independent variables were used to study the mutual effect of various parameters using statistically designed experiments. The experimental ranges and levels of various independent variables in CR removal are given in Table 2. The comparison of predicted response values with experimental results is reported in Table 3.

The analysis of variance (ANOVA) and regression coefficient (R^2) for percentage color removal of CR dye are given in Table 4. The probability level, P, was used to verify the significance of each of the interactions among the factors and T-tests were applied to evaluate the importance of the regression coefficient. Larger values of T and lower values of P ($P < 0.05$) for linear, square, and interaction effects are more significant in the chosen model at the corresponding coefficient terms. The coefficient for the linear effect of X_3 ($P = 0.000$) was the first important factor. X_4 ($P = 0.001$) was the second important factor, and the coefficient for the linear effect of X_1 and X_2 did not signify the effect on color removal. The coefficients of the quadratic effect of X_2, X_3, and X_4 were ($P = 0.000$) the first important factor, while X_1 was the second important factor ($P = 0.006$). The coefficients of the interaction effects of X_2X_4 and X_2X_3 were the first and second important factors ($P = 0.000$, 0.002). However, the coefficients of the other interactive effects (X_1X_2, X_1X_3, X_1X_4, X_3X_4) among the factors did not appear to be significant. The larger value of $F_{statistics}$ indicates that most of the variation in the response can be explained by the regression model equation. The regression model equation (Eq. (5)) for percentage CR dye removal is

$$\begin{aligned}\%\ \text{CR removal} = {} & 96.69 - 0.1333X_1 - 0.1783X_2 + 2.0233X_3 \\ & + 0.4892X_4 - 0.3329X_1^2 - 0.6279X_2^2 - 1.3692X_3^2 \\ & - 1.0654X_4^2 + 0.2337X_1X_2 - 0.2225X_1X_3 - 0.1200X_1X_4 \\ & + 0.5375X_2X_3 + 0.7175X_2X_4 - 0.1787X_3X_4\end{aligned} \quad (5)$$

The regression coefficient, R^2, for the experimental data was 0.9755, which indicates that 97.55% of the variations in response could be described by this model. The adjusted R^2 is a tool to measure the goodness of fit, but it is more suitable for comparing models with different numbers of independent variables. It corrects the R^2 value for the number of terms in the model and the sample size by using the degrees of freedom in its computations. The ANOVA table shows the residual error, which measures the elements of variation in the response that cannot be explained by the model, and their occurrence in a normal distribution. Fig. 8a shows the observed residuals are plotted against the expected values, given by normal distribution. The residuals in the plot follow a straight line and are normally distributed. It can be observed that the residuals from the analysis do not have any effect on the result and are the best residuals. The plot of residual vs. fitted values is shown in Fig. 8b. The residuals in this plot appear to be randomly scattered above and below the zero line. The greater spread of residuals in this plot signifies the increase in the fitted values. Fig. 8c shows the histogram of the residuals. A long tail in the plot indicates the skewed distribution. The one or two bars that are far from the others may be outliers. The non-uniform bars in the plot represent the more fitted values. Fig. 8d illustrates the residuals in the order of the corresponding observations. It was observed that the standardized resid-

Table 2
Experimental range, levels of independent variables for CR dye removal by dual adsorbent

Independent variables	Range and level				
	$-\alpha$	–1	0	1	α
Initial pH (X_1)	5.8	5.9	6.0	6.1	6.2
Initial adsorbate concentration, mg L^{-1} (X_2)	200	250	300	350	400
Wheat bran dosage, g (X_3)	0.5	0.75	1.0	1.25	1.50
Dead cells dosage, g (X_4)	0.1	0.2	0.3	0.4	0.5

Table 3
The 4 factor full factorial central composite design matrix for CR dye removal by dual adsorbent

Run no.	X_1	X_2 (mg L^{-1})	X_3 (g)	X_4 (g)	CR dye removal efficiency (%)	
					Experiment	Predicted
1	α	0	0	0	95.30	95.09
2	0	0	0	α	94.26	93.40
3	0	0	0	0	96.69	96.69
4	$-\alpha$	0	0	0	95.49	95.62
5	0	0	α	0	95.84	95.26
6	–1	–1	–1	–1	92.94	92.06
7	0	0	0	0	96.67	96.69
8	1	1	1	1	95.91	96.46
9	1	1	–1	–1	89.56	89.61
10	1	–1	–1	1	91.85	91.67
11	–1	1	1	–1	94.80	94.65
12	–1	–1	1	–1	95.53	95.83
13	–1	1	1	1	96.28	96.94
14	1	–1	1	–1	94.90	94.89
15	0	0	0	$-\alpha$	90.67	91.45
16	0	0	$-\alpha$	0	86.66	87.16
17	1	–1	–1	–1	92.28	92.01
18	1	–1	1	1	93.25	93.84
19	1	1	–1	1	92.05	92.14
20	–1	–1	1	1	95.64	95.26
21	–1	–1	–1	1	91.45	92.20
22	1	1	1	–1	95.00	94.64
23	0	0	0	0	96.66	96.69
24	0	0	0	0	96.70	96.69
25	0	0	0	0	96.74	96.69
26	0	0	0	0	96.65	96.69
27	–1	1	–1	1	92.06	91.73
28	0	α	0	0	93.96	93.82
29	–1	1	–1	–1	88.92	88.72
30	0	$-\alpha$	0	0	97.35	97.17
31	0	0	0	0	96.72	96.69

Table 4
Analysis of variance (ANOVA) for percentage of CR dye removal using dual adsorbent in 2^4 full factorial central composite design

Term	Coefficient	SE of coefficient	$T_{statistics}$	DF	Seq SS	Adj SS	Adj MS	$F_{statistics}$	Probability
Constant	96.6900	0.2134	453.143						
Regression				14	203.176	203.176	14.5126	45.54	0.000
X_1	0.1333	0.1152	1.157	1	0.427	0.427	0.4267	1.34	0.264
X_2 (mg L^{-1})	0.1783	0.1152	1.548	1	0.763	0.763	0.7633	2.39	0.141
X_3 (g)	2.0233	0.1152	17.558	1	98.253	98.253	98.2531	308.29	0.000
X_4 (g)	0.4892	0.1152	4.245	1	5.743	5.743	5.7428	18.02	0.001
X_1 * X_1	0.3329	0.1056	3.153	1	0.122	3.169	3.1694	9.94	0.006
X_2 (mg L^{-1}) *X_2 (mgL^{-1})	0.6279	0.1056	5.948	1	4.528	11.275	11.2747	35.38	0.000
X_3 (g) * X_3 (g)	1.3692	0.1056	12.969	1	45.614	53.606	53.6061	168.20	0.000
X_4 (g) * X_4 (g)	1.0654	0.1056	10.092	1	32.459	32.459	32.4594	101.85	0.000
X_1 * X_2 (mgL^{-1})	0.2337	0.1411	1.656	1	0.874	0.874	0.8742	2.74	0.117
X_1 * X_3 (g)	0.2225	0.1411	1.577	1	0.792	0.792	0.7921	2.49	0.134
X_1 * X_4 (g)	0.1200	0.1411	0.850	1	0.230	0.230	0.2304	0.72	0.408
X_2 (mg L^{-1}) * X_3 (g)	0.5375	0.1411	3.808	1	4.622	4.622	4.6225	14.50	0.002
X_2 (mg L^{-1}) * X_4 (g)	0.7175	0.1411	5.084	1	8.237	8.237	8.2369	25.84	0.000
X_3 (g) * X_4 (g)	0.1787	0.1411	1.267	1	0.511	0.511	0.5112	1.60	0.223
Residual error				16	5.099	5.099	0.3187		
Lack-of-fit				10	5.093	5.093	0.5093	477.46	0.000
Pure error				6	0.006	0.006	0.0011		
Total				30	208.276				

Regression coefficient R^2 = 0.9755, R^2(Pred) = 0.8591, R^2(adj) = 0.9541
Where SE, standard error of coefficient; DF, degree of freedom; Seq SS, sequential sum of squares; Adj SS, adjusted sum of squares; Adj MS, adjusted mean squares.

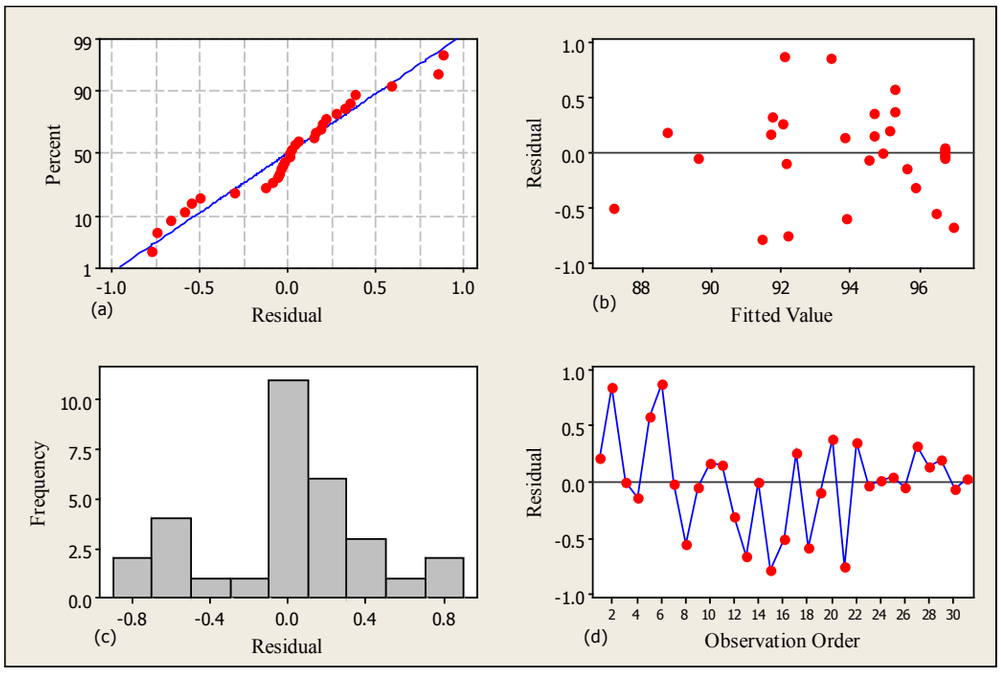

Fig. 8. Residual plots for decolorization of congo red dye by dual adsorbent. (a) Normal probability plot of residuals, (b) Residuals versus fitted values, (c) Frequency of observation versus residuals and (d) Residuals versus the order of the data.

uals fluctuate irregularly around the zero line in the order of observation, and this was used to determine the non-random error [24]

The contour plot between the adsorbate concentration and dead biomass dosage, for percentage color removal, was found to be elliptical, as shown in Fig. 9a. The coordinates of the central point in this plot indicate the optimal value of the respective constituents. The maximum predicted percentage color removal is shown by the minimum curvature of the contour plot, which shows that the highest percentage of color removal from the aqueous solution occurs when the dye concentration ranges between 250 and 350 mg L^{-1} and the dead biomass dosage ranges between 0.25 and 0.4 g. Fig. 9b shows that the maximum percentage color removal occurs when the wheat bran dosage ranges between 1.06 and 1.4 g and pH ranges between 5.8 and 6.15, and the effect is not very significant.

Fig. 10a shows the surface plot of the response variable as a function of pH and wheat bran dosage. It shows that a pH range of 5.8–6.2 does not have significant effect, while a wheat bran dosage between 0.5–1.5 g has a significant effect on the maximum decolorization of the CR dye using the dual adsorbent. Similarly, the surface plot (Fig. 10b) of the dead biomass dosage in the range of 0.1–0.5 g vs. the initial adsorbate concentration in the range of 200–400 mgL^{-1} shows a significant effect on color removal from aqueous solution. The optimal response values obtained from these plots are more similar to the values obtained from the regression model equation. The optimal values of the independent process variables for maximal percentage of color removal are given in Table 5.

3.4. Adsorption isotherm

It is important to find the best fit to the adsorption isotherm to evaluate the efficacy of the prepared dual adsorbent and thus to develop suitable industrial adsorption system designs. The experimental adsorption data were fit by the Freundlich, Langmuir, and Temkin isotherm models. The adsorption on a heterogeneous solid surface and the possibility of multilayer adsorption are expressed by the Freundlich isotherm. It is assumed that the adsorbent-adsorbate interaction decreases with the decrease in available binding sites, as described by the following linear equation [30]

$$\log q_e = \log K_F + \frac{1}{n}\log C_e \quad (6)$$

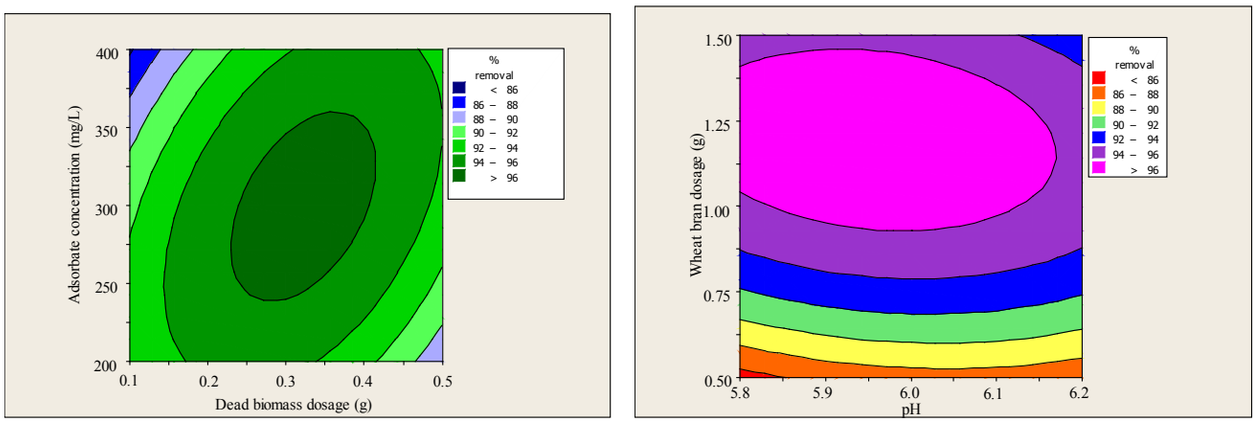

Fig. 9. Contour plots for interactive effect of (a) adsorbate concentration and dead biomass dosage (b) pH and wheat bran dosage on removal of congo red dye.

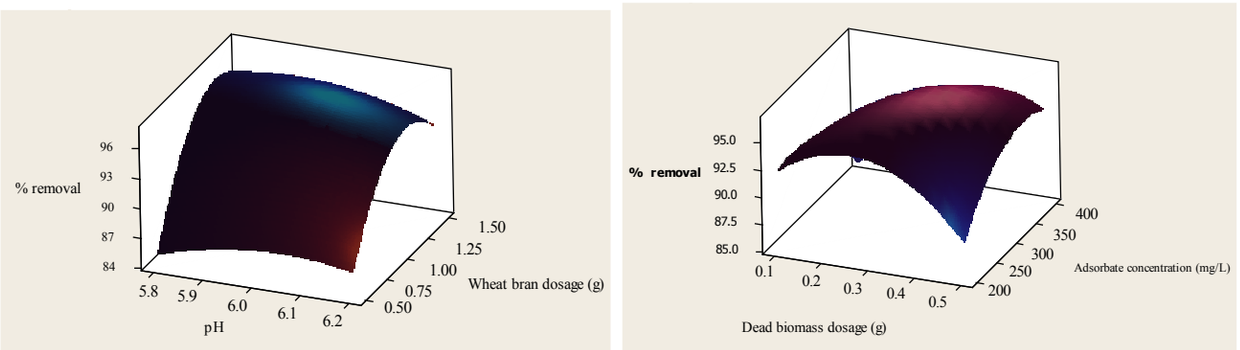

Fig. 10. Surface plots for interactive effect of (a) pH and wheat bran dosage (b) adsorbate concentration and dead biomass dosage on removal of congo red dye.

Table 5
Optimal values of the process parameters for maximum percentage colour removal

Process parameters	Optimum value	CR dye colour removal (%)
Initial pH (X_1)	6	97.35
Initial adsorbate conc. C_o, mg L^{-1} (X_2)	200	
Wheat bran dosage, g (X_3)	1	
Dead biomass dosage, g (X_4)	0.3	

where K_F and $1/n$ are the Freundlich constant (L g^{-1}) and heterogeneity factor, respectively, which indicate the capacity and intensity of adsorption. The plot of log q_e vs. log C_e yields a straight line, of which the slope $1/n$ and intercept K_F are estimated (Fig. 11). The Langmuir isotherm assumes that the adsorbed layer is unimolecular. According to this isotherm, an active binding site becomes inactive once a dye molecule is adsorbed onto it. For solid-liquid systems, the linearized Langmuir equation is written as [31]

$$\frac{1}{q_e} = \frac{1}{q_{\max}} + \frac{1}{q_{\max} K_L C_e} \tag{7}$$

where K_L is the Langmuir constant (L mg^{-1}) and q_m is the maximum saturation capacity corresponding to the monolayer coverage on the surface (mg g^{-1}). The linear plot of $1/q_e$ vs. $1/C_e$ permits the determination of the maximum saturation capacity and Langmuir constant from the intercept and slope of the plot (Fig. 12). A further study of this equation was made by introducing a dimensionless constant called the separation factor, R_L, also known as the equilibrium parameter and stated by [32].

$$R_L = \frac{1}{1 + K_L C_o} \tag{8}$$

$R_L > 1$, $R_L = 1$, $0 < R_L < 1$ and $R_L = 0$ indicate unfavorable, linear, favorable, and irreversible types of isotherms, respectively. The Temkin isotherm is based on the assumption that the heat of adsorption decreases linearly as adsorbate-adsorbate interactions increase. It is given by the following linear equation [33]

$$q_e = \frac{RT}{b_T} \ln K_T + \frac{RT}{b_T} \ln C_e \tag{9}$$

where K_T (L mg^{-1}) is the Temkin isotherm constant, RT/b_T indicates the heat of adsorption, and T and R are the absolute temperature (K) and the universal gas constant (J $mole^{-1}$ K^{-1}), respectively. The plot of q_e vs. ln C_e is used to determine the isotherm constants b_T and K_T from the slope and intercept (Fig. 13).

3.5. Inference from adsorption isotherm models

The adsorption isotherms results are shown in Table 6. A higher value of the regression coefficient ($R^2 = 0.992$) was found in the Langmuir model, compared to the Freundlich ($R^2 = 0.944$) and Temkin isotherm ($R^2 = 0.969$) models. Hence the equilibrium adsorption data followed Langmuir isotherm model. According to the assumptions of the Langmuir isotherm, the adsorption of CR dye onto the dual adsorbent was homogeneous in nature with the formation of monolayer at active sites[22,34].The maximum monolayer capacity of the dual adsorbent (q_{max}) was determined to be 46.3 mg g^{-1}. This proves that 1 g of the prepared dual adsorbent could adsorb 46.3 mg of CR dye. Similarly, the maximum monolayer adsorption capacities of various adsorbents for

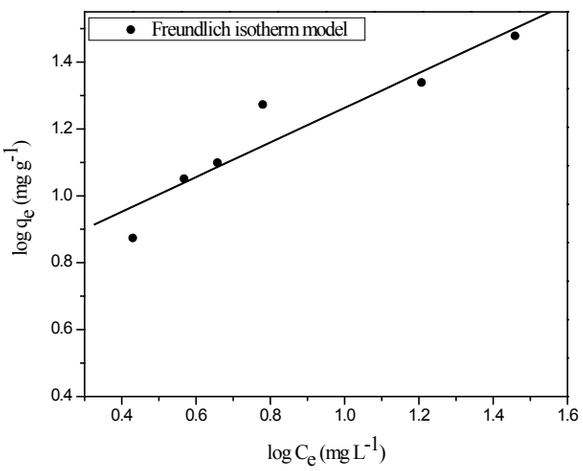

Fig. 11. Freundlich isotherm plot for adsorption of CR dye onto dual adsorbent.
(pH: 6; adsorbate concentration: 100–400 mg L^{-1}; wheat bran dosage: 10 g L^{-1}; dead biomass dosage: 3 g L^{-1}; agitation speed: 200 rpm; Temperature: 303 K; contact time: 24 h).

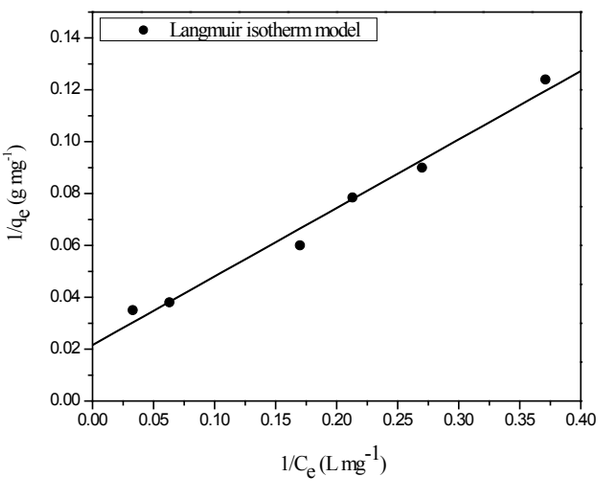

Fig. 12. Langmuir isotherm plot for adsorption of CR dye onto dual adsorbent.
(pH: 6; adsorbate concentration: 100–400 mg L^{-1}; wheat bran dosage: 10 g L^{-1}; dead biomass dosage: 3 g L^{-1}; agitation speed: 200 rpm; Temperature: 303 K; contact time: 24 h).

the removal of CR dye was reported in Table 7. It can be inferred from the table that the prepared dual adsorbent had superior adsorption property for the removal of CR dye on comparison with the reported adsorbents.

3.6. Thermodynamic parameters

The thermodynamic parameters for the adsorption of CR dye were determined using the following equation [9,22]

$$\Delta G = RT \ln(K_a) \tag{10}$$

$$\ln K_a = \frac{\Delta S_{ads}}{R} - \frac{\Delta H_{ads}}{RT} \tag{11}$$

The thermodynamic parameters, such as the change in Gibbs free energy (ΔG), change in enthalpy (ΔH), and change in entropy (ΔS) of the process, were determined from the adsorption equilibrium constant K_a (= q_{max} K_L)[9]. The activation energy (E_a) for the adsorption of CR onto the dual adsorbent was determined using the Arrhenius equation. The linear form of the Arrhenius equation is expressed as [47]

$$\ln K = \ln A - \left(\frac{E_a}{RT}\right) \tag{12}$$

where A is the Arrhenius frequency factor, T is the adsorption temperature (K), and K is the pseudo-second-order rate constant (K_2) obtained for each reaction performed at 303 K to 328 K, using 300 mg L^{-1} dye solutions. The thermodynamic parameters were calculated by plotting ln K_a vs. 1/T

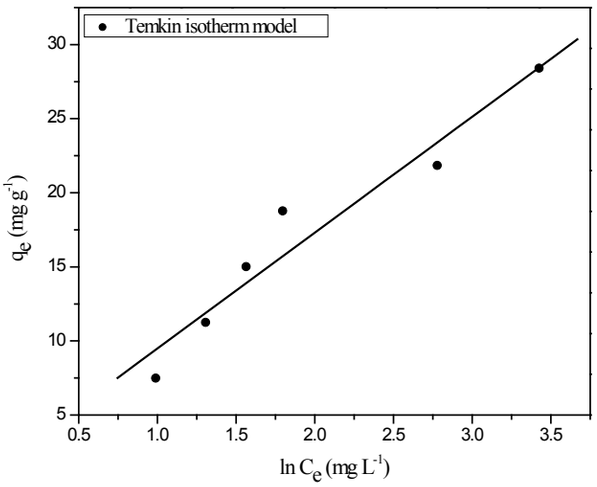

Fig. 13. Temkin isotherm plot for adsorption of CR dye onto dual adsorbent.
(pH: 6; adsorbate concentration: 100–400 mg L^{-1}; wheat bran dosage: 10 g L^{-1}; dead biomass dosage: 3 g L^{-1}; agitation speed: 200 rpm; Temperature: 303 K; contact time: 24 h).

Table 7
Comparison of maximum CR dye adsorption capacity of various adsorbents determined by Langmuir adsorption isotherm model

Adsorbent	Maximum adsorption capacity q_m (mg g^{-1})	Reference
Zeolite	3.77	[35]
Waste red mud	4.05	[36]
Kaolin	5.44	[35]
Activated carbon from coir pith	6.70	[37]
Acid activated red mud	7.08	[38]
Bagasse fly ash	11.88	[39]
Montmorillonite	12.70	[40]
Orange Peel	14.00	[41]
Rice bran	14.63	[42]
Aspergillus niger	14.72	[16]
Banana peel	18.20	[41]
Orange Peel	22.44	[43]
Anilinepropylsilica xerogel	22.62	[44]
Wheat bran	22.73	[42]
Apricot stone activated carbon	32.85	[45]
Jute stick powder	35.70	[46]
Sodium bentonite	35.84	[35]
Neem Leaf powder	41.24	[12]
Neurospora crassa dead biomass with wheat bran	46.29	Present work

Table 6
Adsorption isotherms constants for CR dye adsorption onto dual adsorbent

Isotherm	Freundlich			Langmuir			Temkin		
	n	K_F (L g^{-1})	R^2	q_m (mg g^{-1})	K_L (L mg^{-1})	R^2	K_T (L mg^{-1})	B_T	R^2
Model parameters	1.931	5.564	0.944	46.296	0.08175	0.992	1.239	322.22	0.969
Model Equation		$q_e = 5.5637\ C_e^{1.931}$			$q_e = \frac{3.7851 C_e}{1+0.08175 C_e}$			$q_e = 7.818 \ln (1.239\ C_e)$	

(Fig. 14), and the values are reported in Table 8. The effect of temperature on CR dye uptake by the dual adsorbent is shown in Fig. 15, which shows that the amount of dye adsorbed, q_e (mg g^{-1}) increases with the increase in temperature. The maximum adsorption capacity, q_m, of the 300 mg L^{-1} CR dye solution increased from 46.29 mg g^{-1} at 303 K to 109.890 mg g^{-1} at 328 K, at equilibrium times of 8 h and 5 h, respectively. This is because the pore sizes of the dual adsorbent particles were enlarged at raised temperatures [9]. The pore volume was observed to increase from 1.8 mm^3 g^{-1} at room temperature to 3.3 mm^3 g^{-1} at 328 K. Table 8 shows that the values of ΔG decreased with the increase in temperature, indicating that the adsorption was a spontaneous process. The positive value of ΔH indicates that the adsorption of CR onto the dual adsorbent was an endothermic process. The positive value of ΔS suggests increased randomness of dye molecules on the dual adsorbent surface than in the dye solution. The activation energy of adsorption, determined from the slope of the linear plot of ln K vs. 1/T, was found to be 42.78 kJ mole^{-1} with an adsorbate concentration of 300 mg L^{-1}. This value of activation energy indicates a chemisorptive process. The activation energy for chemisorption was between 40–800 kJ mole^{-1}, confirming the stronger bonding forces acting between CR dye molecules and active sites on the dual adsorbent at higher temperature [47,10].

3.7. Kinetic studies of adsorption

Kinetic studies for the adsorption of CR dye onto the dual adsorbent was carried out for different initial adsorbate concentrations ranging from 50 to 300 mg L^{-1}. It was observed that the dye uptake rate was fast in the beginning stages of the adsorption process. However, the dye removal rate later decreased gradually with time. The CR dye attained its equilibrium adsorption capacity at approximately 2 h for 50 mg L^{-1}, 3 h for 100 mg L^{-1}, 4 h for 150 mg L^{-1}, 6 h for 200 mg L^{-1}, 7 h for 250 mg L^{-1} and 8 h for 300 mg L^{-1}.

Kinetic models were used to find the rate constants of the adsorption process. Kinetic data were fitted with Lagergren pseudo-first-order [48] and Ho's second-order [49] kinetic models. The mathematical representations of pseudo-first-order and pseudo-second-order model equations are given in Eqns. (13) and (14), respectively,

$$\ln(q_e - q_t) = \ln q_e - K_1 t \tag{13}$$

where q_e and q_t are the solid-phase adsorbate concentrations (mg g^{-1}) at equilibrium and at any time t (min), and K_1 is the rate constant of pseudo-first-order adsorption (min^{-1}). The values of q_e and K_1 can be obtained from the intercept and slope of the plot of ln ($q_e - q_t$) vs. t. The linear form of pseudo-second-order kinetic equation is expressed as

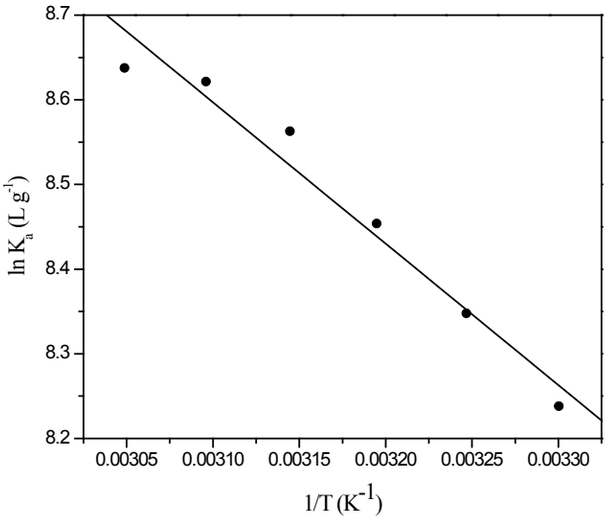

Fig. 14. Van't Hoff plot for adsorption of CR dye onto dual adsorbent.
(pH: 6; adsorbate concentration: 100–400 mg L^{-1}; wheat bran dosage: 10 g L^{-1}; dead biomass dosage:3 g L^{-1}; agitation speed: 200 rpm; contact time: 24 h).

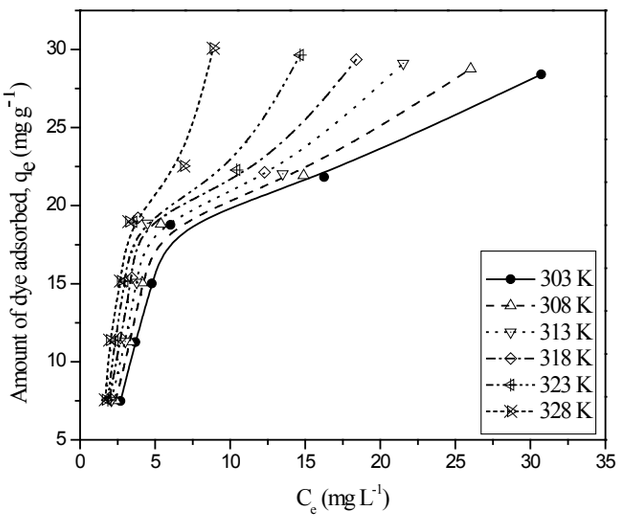

Fig. 15. Effect of temperature on adsorption of CR dye onto dual adsorbent.
(pH: 6; adsorbate concentration: 100–400 mg L^{-1}; wheat bran dosage: 10 g L^{-1}; dead biomass dosage: 3 g L^{-1}; agitation speed: 200 rpm; contact time: 24 h).

Table 8
Thermodynamic parameters for the adsorption of CR dye onto dual adsorbent

Initial adsorbate conc. (mg L^{-1})	ΔG (kJ mole^{-1})						ΔH (kJ mole^{-1})	ΔS (kJ mole^{-1} K^{-1})
	303 K	308 K	313 K	318 K	323 K	328 K		
300	–20.755	–21.376	–21.999	–22.639	–23.152	–23.554	13.88	0.1144

$$\frac{t}{q_t} = \frac{1}{K_2 q_e^2} + \frac{t}{q_e} \tag{14}$$

The pseudo-second-order kinetic rate constant was determined from the linear plot of t/q_t vs. t. The initial rate of adsorption h (mg g^{-1} min^{-1}) is described by [10]

$$h = K_2 q_{e^2} \tag{15}$$

where K_2 is the equilibrium rate constant of pseudo-second-order adsorption (g mg^{-1} min^{-1}).

3.8. Inference from adsorption kinetic models

The plots for pseudo-first-order and pseudo-second-order models were shown in Figs. 16 and 17 respectively. Kinetic model parameters determined from these plots were given in Table 9. The higher R^2 values (close to 1) of pseudo-second-order model and the close agreement between its predicted $q_{e,calc}$ and experimental $q_{e,expt}$ values indicates that the adsorption kinetic data followed pseudo-second-order model. Since the kinetic studies were well explained by pseudo second-order model, it can be assumed that the sorption of CR dye onto dual adsorbent was a chemisorption process. The adsorption experiments were carried out at pH 6. The zero point charge of the dual adsorbent was found to be at pH 9. Therefore at pH 6, the surface of the dual adsorbent will be positively charged which facilitates the binding of negatively charged anionic dye. Hence the adsorption of CR dye onto dual adsorbent was chemisorption involving strong valence forces through sharing or the ion exchange of electrons between the adsorbent and adsorbate molecules as covalent forces [22, 25]. The chemisorption mechanism which is involved in the studied adsorption process was further confirmed by the activation energy as discussed in section 3.6. The rate constant, K_2, decreased from 0.151 to 0.02 g mg^{-1} min^{-1} as the dye concentration was increased from 50 to 300 mg L^{-1}. This is because of the decreased competition for the binding sites at lower concentrations and increased competition at the surface sites of the dual adsorbent at higher concentrations [29].

3.9. Adsorption mechanism

While designing a solid-liquid adsorption system, the dye molecule transfer and rate of adsorption are explained by either an external boundary film, pore diffusion, or both. These phenomena can be explained by the following steps. [22,50]

a) Transfer of dye molecules from bulk dye solution through the liquid film to the outer layer of the adsorbent.
b) Internal diffusion, the transport of dye molecules from the particle surface into inner sites on the pores of the adsorbent.
c) Adsorption of dye molecules from the binding sites into the inner surface of the pores and capillary spaces of the adsorbent.

The diffusion mechanism of adsorption is explained by the intra-particle diffusion (pore diffusion) model. This model is represented by the equation [50]

$$q_t = K_i t^{0.5} + C \tag{16}$$

where K_i is the pore diffusion rate constant (mg g^{-1} $min^{-1/2}$) and C is the constant. The thickness of the boundary film

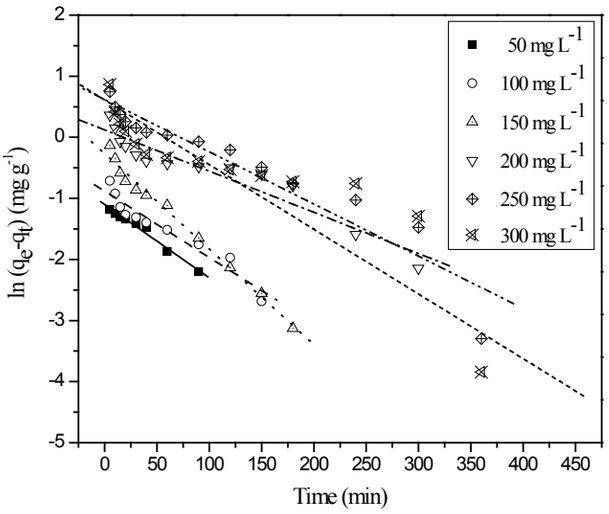

Fig. 16. Lagergren pseudo-first-order kinetic plotfor adsorption of CR dye onto dual adsorbent.
(pH: 6; adsorbate concentration: 50–300 mg L^{-1}; wheat bran dosage: 10 g L^{-1}; dead biomass dosage: 3 g L^{-1}; agitation speed: 200 rpm; Temperature: 303 K; contact time: 24 h).

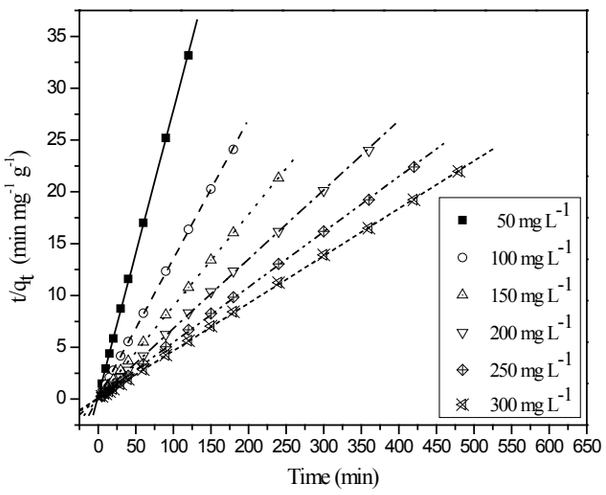

Fig. 17. Ho's pseudo-second-order kinetic plot for adsorption of CR dye onto dual adsorbent.
(pH: 6; adsorbate concentration: 50–300 mg L^{-1}; wheat bran dosage: 10 g L^{-1}; dead biomass dosage: 3 g L^{-1}; agitation speed: 200 rpm; Temperature: 303 K; contact time: 24 h).

Table 9
Kinetic parameters for the adsorption of CR dye onto dual adsorbent

Initial adsorbate conc. (mg L^{-1})	$q_{e'expt}$ (mg g^{-1})	Pseudo-first-order model			Pseudo-second-order model				Intra-particle diffusion model		
		$q_{e'calc}$ (mg g^{-1})	K_1 (min^{-1})	R^2	$q_{e'calc}$ (mg g^{-1})	h (mg g^{-1} min^{-1})	K_2 (g mg^{-1} min^{-1})	R^2	K_i (mg g^{-1} $min^{-1/2}$)	C	R^2
50	3.68	0.333	0.0120	0.979	3.697	2.064	0.151	0.999	0.0295	3.293	0.982
100	7.49	0.413	0.0108	0.964	7.480	3.482	0.062	0.999	0.0334	6.988	0.967
150	11.25	0.765	0.0156	0.983	11.295	4.531	0.035	0.999	0.0537	10.477	0.942
200	15.02	1.128	0.0067	0.942	15.053	5.739	0.025	0.999	0.0618	13.784	0.954
250	18.77	1.856	0.0085	0.951	18.800	6.385	0.018	0.999	0.0927	16.925	0.966
300	21.84	1.843	0.0105	0.907	21.891	9.584	0.020	0.999	0.0742	20.281	0.883

is given by the value of C. The values of K_i and C are determined from the slope and intercept, respectively, of the linear plot of q_t vs. $t^{1/2}$. The Boyd kinetic expression is used to predict the slowest step, which is the rate-limiting step in the adsorption. It is described by the following equation [22,29]

$$R_t = -0.4977 - \ln(1 - F) \quad (17)$$

$$F = \frac{q_t}{q_e} \quad (18)$$

where q_t is the amount of CR adsorbed at time t (mg g^{-1}), F is the ratio of solute adsorbed at any time t, and B_t is a mathematical function of F.

The intra-particle diffusion plot for the adsorption of CR onto the dual adsorbent is shown in Fig. 18. From the intra-particle diffusion plot 18, the first linear portion follows the external mass transfer diffusion of the adsorbate and the second linear portion follows pore diffusion effects. Extrapolation of the second linear portion back to the y axis gives the value of C. A larger external film diffusion effect is indicated by a large intercept value. A smaller intercept value denotes that the adsorption process is mostly governed by pore diffusion, with a slight effect of boundary layer diffusion. According to the data in Table 9, the coefficients of regression, R^2, of the pore diffusion model for different adsorbate concentrations were lower than those for the pseudo-second-order kinetic model. These proved that the experimental data were well-fitted with the pseudo-second-order kinetic model. Therefore, the overall rate of the adsorption is mostly governed by external film diffusion, followed by a minor effect of pore diffusion of dye anions to the inner surface. The Boyd kinetic expression was used to further analyze the adsorption kinetic data. The Boyd plot (Fig. 19) was found to be a straight line that did not pass through the origin. This suggests that external film diffusion mainly controls the rate of the reaction.

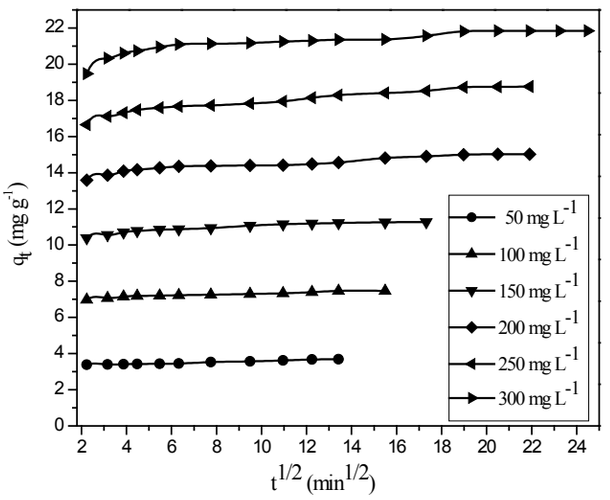

Fig. 18. Intra-particle diffusion plot for adsorption of CR dye onto dual adsorbent.
(pH: 6; adsorbate concentration: 50–300 mg L^{-1}; wheat bran dosage: 10 g L^{-1}; dead biomass dosage: 3 g L^{-1}; agitation speed: 200 rpm; Temperature: 303 K; contact time: 24 h).

3.10. Comparison of adsorption efficiency of individual adsorbents and dual adsorbent

The batch experiments for the removal of CR dye were carried out with individual adsorbents in separate batches for comparison purpose. The initial CR dye concentration was fixed as 300 mg L^{-1} and was treated with 13 g L^{-1} of wheat bran and *Neurospora crassa* dead biomass in separate batches. The percentage color removal was calculated for regular time intervals and compared with the adsorption efficiency of the dual adsorbent (10 g L^{-1} of wheat bran and 3 g L^{-1} of *Neurospora crassa* dead biomass). The results were illustrated in Fig. 20. It was observed that the dual adsorbent had better adsorption efficiency when compared to the individual adsorbents.

3.11. Desorption studies and reusability of dual adsorbent

To economize the adsorption process, desorption experiments were performed for the recovery of the dual adsorbent. The amount of CR dye desorbed decreased with an increasing number of runs. It was found that up to a maximum of 56.3% of the dye could be desorbed using the solvent methanol in the 3rd run, compared with other desorbing agents that are useful for industrial purposes. The regener-

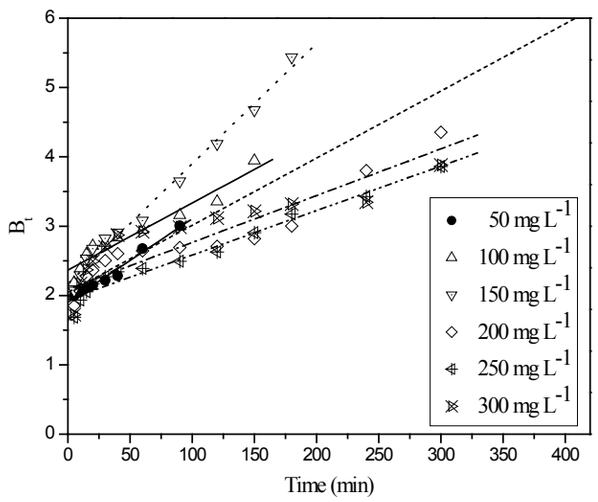

Fig. 19. Boyd plot for adsorption of CR dye onto dual adsorbent. (pH: 6; adsorbate concentration: 50–300 mg L^{-1}; wheat bran dosage: 10 g L^{-1}; dead biomass dosage: 3 g L^{-1}; agitation speed: 200 rpm; Temperature: 303 K; contact time: 24 h).

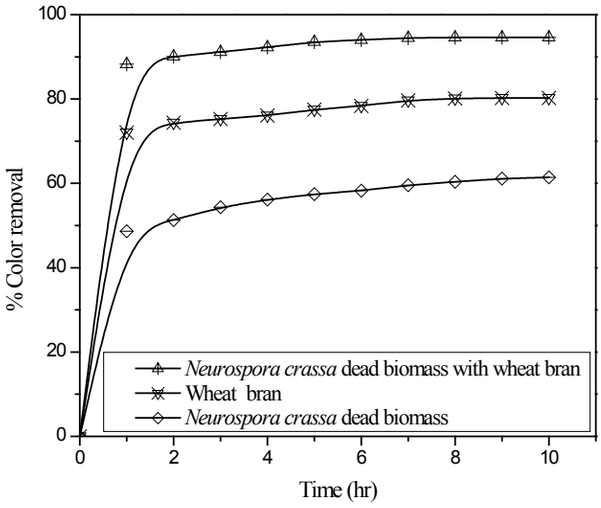

Fig. 20. Comparison of adsorption efficiency of individual adsorbents and dual adsorbent.
(pH 6; adsorbate concentration: 300 mg L^{-1}; dual adsorbent dosage: 13 g L^{-1} (wheat bran 10 g and dead biomass dosage 3 g); adsorbent wheat bran dosage: 13 g L^{-1}; adsorbent dead biomass dosage 13 g L^{-1}; agitation speed: 200 rpm; Temperature: 303 K; contact time: 10 h).

ated dual adsorbent was added to the optimized adsorbate solution of concentration 300 mg L^{-1}. The regenerated dual adsorbent was tested in the 2nd and 3rd runs. In comparison to the 1st run, 81.3% adsorption was maintained after 24 h in the 2nd run and 70.2% in the 3rd run, which may be due to the incomplete desorption of the bound dye anions from the dual adsorbent active sites and lack of active sites on the dual adsorbent. Therefore, the dye adsorption percentage decreased with the increase in the number of runs.

4. Conclusion

It was found that the filamentous dead fungus *Neurospora crassa* along with wheat bran may be used as an adsorbing material for decolorization of CR dye from an aqueous solution. Additionally, the fungus was found to be free from pathogenicity. The various influencing factors, such as pH, initial adsorbate concentration, wheat bran dosage, and dead biomass dosage, were optimized using factorial experimental design. The peaks in FT-IR revealed that the surface of the dual adsorbent material contains abundant hydroxyl, methyl, and carbonyl groups. The experimental equilibrium data were in good agreement with the Langmuir isotherm model, confirming the monolayer adsorption of CR onto the dual adsorbent. Thermodynamic parameters, that is, the negative value of ΔG and the positive value of ΔH, confirmed that the process is spontaneous and endothermic in nature and, thus, the adsorption is favorable at higher temperatures and occurs via chemisorption. Kinetic experiments revealed that the adsorption followed a pseudo-second-order rate equation. It was found that external film diffusion controlled the dye uptake in the earlier stages, followed by pore diffusion, which controlled the rate at later stages. The Boyd plot confirmed that the external film diffusion is the slowest step that mainly governs the rate of the reaction. The maximum percentage of CR dye could be desorbed using the solvent methanol in desorption experiments. The regenerated dual adsorbent can be used effectively up to three cycles to adsorb CR dye in aqueous solutions. It was concluded from the results that the prepared material was a useful dual adsorbent for effective decolorization of anionic dyes from industrial effluents.

References

[1] C. Srilakshmi, R. Saraf, Agdoped hydroxyapatite as efficient adsorbent for removal of congo red dye from aqueous solutions: synthesis, kinetic and equilibrium adsorption isotherm analysis, Micropor. Mesopor. Mater., 219 (2016) 134–144.
[2] S. Saantos, R. Boaventura, Treatment of a simulated textile wastewater in a sequencing batch reactor with addition of a low–cost adsorbent, J. Hazard. Mater., 291 (2015) 74–82.
[3] E.M. Saggioro, A.S. Oliveria, D.F. Buss, D.P. Magalhaes, T. Pavesi, M. Jimenez, M.I. Maldonado, L.F.V. Ferreira, J.C. Moreira, Photo–decolorization and ecotoxicological effects of solar compound parabolic collector pilot plant and artificial light photocatalysis of indigo carmine dye, Dyes Pigments, 113 (2015) 571–580.
[4] S.R. Couto, Dye removal by immobilized fungi, Biotechnol. Adv., 27 (2009) 227–235.
[5] S. Chatterjee, D.S. Lee, M.W. Lee, S.H. Woo, Enhanced adsorption of congo red from aqueous solutions by chitosan hydrogel beads impregnated with cetyl trimethyl ammonium bromide, Biores. Technol., 100 (2009) 2803–2809.
[6] G. Crini, Non-conventional low cost adsorbents for dye removal: a review, Biores. Technol., 97 (2006) 1061–1085.
[7] A. Srinivasn, T. Viraraghavan, Decolorization of dye wastewaters by biosorbents: A review, J. Environ. Manage., 91 (2010) 1915–1929.
[8] A. Banerjee, P. Sarkar, S. Banerjee, Application of statistical design of experiments for optimization of As(V) biosorption by immobilized bacterial biomass, Ecol. Eng., 86 (2016) 13–23.
[9] M.T. Sulak, E. Demirbas, M. Kobya, Removal of astrazon yellow 7GL from aqueous solutions by adsorption onto wheat bran, Biores. Technol., 98 (2007) 2590–2598.

[10] X. Han, W. Wang, X. Ma, Adsorption characteristics of methylene blue onto low cost biomass material lotus leaf, Chem. Eng. J., 171 (2011) 1–8.
[11] Y.S. Ho, G. McKay, Sorption of dyes and copper ions onto biosorbents, Process Biochem., 38 (2003) 1047–1061.
[12] K.G. Bhattacharyya, S. Arunima, *Azadirachta indica* leaf powder as an effective biosorbent for dyes: a case study with aqueous congo red solutions, J. Environ. Manage., 71 (2004) 217–229.
[13] R. Han, D. Ding, Y. Xu, W. Zou, Y. Wang, Y. Li, L. Zou, Use of rice husk for the adsorption of congo red from an aqueous solution in column mode, Biores. Technol., 99 (2008) 2938–2946.
[14] R. Gong, S. Zhu, D. Zhang, J. Chen, S. Ni, R. Guan, Adsorption behavior of cationic dyes on citric acid esterifying wheat straw: kinetic and thermodynamic profile, Desalination, 230 (2008) 220–228.
[15] M. Iqbal, A. Saeed, Biosorption of reactive dye by loofa sponge-immobilized fungal biomass of *Phanerochaete chrysosporium*, Process Biochem., 42 (2007) 1160–1164.
[16] Y. Fu, T. Viraraghavan, Removal of congo red from an aqueous solution by fungus *Aspergillus niger*, Adv. Environ. Res., 7 (2002) 239–247.
[17] T. O'Mahony, E. Guibal, J.M. Tobin, Reactive dye biosorption by *Rhizopus arrhizus* biomass, Enzyme Microb. Tech., 31 (2002) 456–463.
[18] G. Bayramoglu Gulay, M.Y. Arica, Biosorption of benzidine based textile dyes "Direct blue 1 and Direct red 128" using native and heat-treated biomass of *Trametes versicolor*, J. Hazard. Mater., 143 (2007) 135–143.
[19] D. Asma, S. Kahraman, S. Cing, O. Yesilada, Adsorptive removal of textile dyes from aqueous solutions by dead fungal biomass, J. Basic Microbiol., 46 (2006) 3–9.
[20] T. Akar, T.A. Demir, I. Kiran, A. Ozcan, A.S. Ozcan, S. Tunali, Biosorption potential of *Neurospora crassa* cells for decolorization of Acid Red 57 dye, J. Chem. Technol. Biotechnol., 81 (2006) 1100–1106.
[21] S. Preethi, A. Sivasamy, S. Sivanesan, V. Ramamurthi, G. Swaminathan, Removal of safranin basic dye from aqueous solutions by adsorption onto corncob activated carbon, Ind. Eng. Chem. Res., 45 (2006) 7627–7632.
[22] S. Nethaji, A. Sivasamy, G. Thennarasu, S. Saravanan, Adsorption of malachite green dye onto activated carbon derived from *Borassus aethiopum* flower biomass, J. Hazard. Mater., 181 (2010) 271–280.
[23] K. Ravikumar, K. Pakshirajan, T. Swaminathan, K. Balu, Optimization of batch process parameters using response surface methodology for dye removal by a novel adsorbent, Chem. Eng. J., 105 (2005) 131–138.
[24] M.B. Kasiri, A.R. Khataee, Photooxidative decolorization of two organic dyes with different chemical structures by UV/H_2O_2 process: Experimental design, Desalination, 270 (2011) 151–159.
[25] A. Sivasamy, S. Nethaji, J.L. Nisha, Equilibrium, kinetic and thermodynamic studies on the biosorption of reactive acid dye on *Enteromorpha flexuosa* and *Gracilaria corticata*, Environ. Sci. Pollut. Res., 19 (2012) 1687–1695.
[26] D. Park, Y.S. Yun, J.M. Park, The past, present and future trends of biosorption, Biotechnol. Bioprocess Eng., 15 (2010) 86–102.
[27] C. Somasekhara Reddy, Removal of direct dye from aqueous solutions with an adsorbent made from tamarind fruit shell, an agricultural solid waste, J. Sci. Ind. Res., 65 (2006) 443–446.
[28] N.K. Amin, Removal of reactive dye from aqueous solutions by adsorption onto activated carbons prepared from sugarcane bagasse pith, Desalination, 223 (2008) 152–161.
[29] V. Vadivelan, K. Vasanth Kumar, Equilibrium, kinetics, mechanism, and process design for the sorption of methylene blue onto rice husk, J. Colloid Interface Sci., 286 (2005) 90–100.
[30] H.M.F. Freundlich, Over the adsorption in solution, J. Phys. Chem., 385 (1906) 385–470.
[31] I. Langmuir, The adsorption of gases on plane surfaces of glass, mica and platinum, J. Am. Chem. Soc., 40 (1918) 1361–1403.
[32] K.R. Hall, L.C. Eagleton, A. Acrivos, T. Vermeulen, Pore and solid diffusion kinetics in fixed-bed adsorption under constant pattern conditions, Ind. Eng. Chem. Fundamn., 5 (1966) 212–223.
[33] M.J. Temkin, V. Pyzhev, Kinetics of ammonia synthesis on promoted iron catalysts, Acta Physicochim. U.R.S.S., 12 (1940) 217–222.
[34] P. Muthamilselvi, R. Karthikeyan, B.S.M. Kumar, Adsorption of phenol onto garlic peel: optimization, kinetics, isotherm, and thermodynamic studies, Desal. Water Treat., 57 (2016) 2089–2103.
[35] V. Vimonses, S. Lei, B. Jina, C.W.K. Chowd, C. Saint, Kinetic study and equilibrium isotherm analysis of congo red adsorption by clay materials, Chem. Eng. J., 148 (2009) 354–364.
[36] C. Namasivayam, D.J.S.E. Arasi, Removal of congo red from wastewater by adsorption onto waste red mud, Chemosphere, 34 (1997) 401–417.
[37] C. Namasivayam, D. Kavitha, Removal of congo red from water by adsorption onto activated carbon prepared from coir pith, an agricultural solid waste, Dyes Pigments, 54 (2002) 47–58.
[38] A. Tor, Y. Cengeloglu, Removal of congo red from aqueous solution by adsorption onto acid activated red mud. J. Hazard. Mater., 138 (2006) 409–415.
[39] I.D. Mall, V.C. Srivastava, N.K. Agarwal, I.M. Mishra, Removal of congo red from aqueous solution by bagasse fly ash and activated carbon: Kinetic study and equilibrium isotherm analyses, Chemosphere, 61 (2005) 492–501.
[40] L. Wang, A. Wang, Adsorption characteristics of congo red onto the chitosan/montmorillonite nanocomposite, J. Hazard. Mater., 147 (2007) 979–985.
[41] G. Annadurai, R. Juang, D. Lee, Use of cellulose-based wastes for adsorption of dyes from aqueous solutions, J. Hazard. Mater., B92 (2002) 263–274.
[42] X.S. Wang, J.P. Chen, Biosorption of congo red from aqueous solution using wheat bran and rice bran: batch studies, Sep. Sci. Technol., 44 (2009) 1452–1466.
[43] C. Namasivayam, N. Muniasamy, K. Gayatri, M. Rani, K. Ranganathan, Removal of dyes from aqueous solutions by cellulosic waste orange peel. Biores. Technol., 57 (1996) 37–43.
[44] F.A. Pavan, S.L.P. Dias, E.C. Lima, E.V. Benvenutti, Removal of congo red from aqueous solution by anilinepropylsilica xerogel, Dyes Pigm., 76 (2008) 64–69.
[45] M. Abbasa, M. Trari, Kinetic, equilibrium and thermodynamic study on the removal of congo red from aqueous solutions by adsorption onto apricot stone, Process Saf. Environ., 98 (2015) 424–436.
[46] G.C. Panda, S.K. Das, A.K. Guha, Jute stick powder as a potential biomass for the removal of congo red and rhodamine B from their aqueous solution, J. Hazard. Mater., 164 (2009) 374–379.
[47] L. Abramian, H. EI-Rassy, Adsorption kinetics and thermodynamics of azo-dye orange II onto highly titania aerogel, Chem. Eng. J., 150 (2009) 403–410.
[48] S. Lagergren, Zur theorie der sogenannten adsorption geloster stoffe, Kungliga svenska vetenskapsakademiens, Handlingar, 24 (1898) 1–39.
[49] Y.S. Ho, G. McKay, Pseudo-second order model for sorption processes, Process Biochem., 34 (1999) 451–465.
[50] A. Gurses, C. Dogar, M. Yalcin, M. Acikyildiz, R. Bayrak, S. Karaca, The adsorption kinetics of the cationic dye, methylene blue, onto clay, J. Hazard. Mater., B131 (2006) 217–228.

Supplementary information

Smart Instruments

Pore Volume Analyser	**Model: Smart Sorb 92/93**
From Smart Instruments Co.Pvt.Ltd.	**WebSite: www.smartinstrument.com**
Run Time:03:03 pm	Date:August 4 2016
% of N2 :95.03	Room temp in Deg C:25
Sample Name : 2 untreated	
Wt of Tube (gms) :24.298	Wt of Tube+Sample (gms) :24.942
Sample Wt (gms) : .6440	Sample Wt after Reg. (gms) : .6430
Sample Loss : .2 %	
Regeneration Temp (deg C) : 30	
Time for regeneration (min.) :120	
Desorption count : 615	
Injection count : 140.3624	
Injected volume (cc) : 0.2	

Pore Volume in (cc/gm) : 0.0018

Remarks: | | |

Fig. S1. Pore volume of dual adsorbent at 303 K.

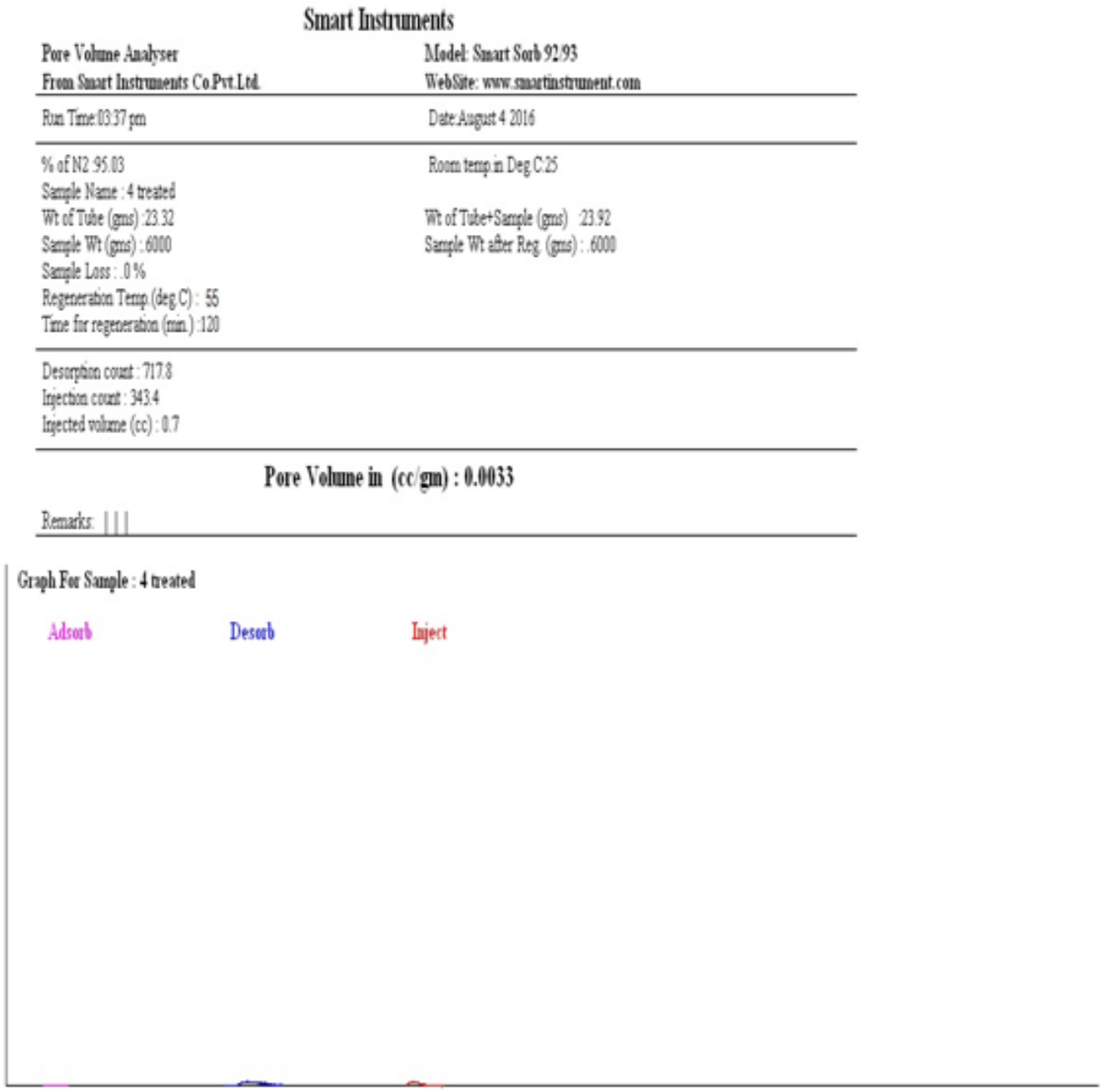

Fig. S2. Pore volume of dual adsorbent at 328 K.

Table S1
Desorption studies for the removal of CR dye from the dual adsorbent in various runs (Volume of desorbing agent: 100 ml; shaking speed: 200 rpm; Temperature: 303 K; contact time: 24 h)

Sl. No	Desorbing agent	% removal of CR dye from the dual adsorbent in the desorption studies		
		1st run	2nd run	3rdrun
1	Ethanol	76.403	64.485	30.904
2	Methanol	87.541	80.450	56.276
3	IPA	21.591	12.204	5.771
4	1 M NaOH	75.335	58.606	24.612
5	Acetone	57.269	44.766	19.884
6	H_2O	47.415	35.794	17.925
7	1 M $CaCl_2$	1.114	0.488	0.315
8	1 M NH_4OH	34.118	22.784	11.556
9	1 M Na_2CO_3	1.627	0.216	0.070
10	1 M $NaHCO_3$	0.771	0.259	0.156
11	0.1 M NaOH	64.078	40.047	16.488

Table S2
Reusability of dual adsorbent for the adsorption of CR dye in various runs (pH: 6; adsorbate concentration: 300 mg L^{-1}; agitation speed: 200 rpm; Temperature: 303 K; contact time: 24 h)

Sl. No	Desorbing agent	% adsorption of CR dye by regenerated dual adsorbent		
		1st run	2nd run	3rd run
1	Ethanol	93.850	69.373	44.695
2	Methanol	93.877	81.297	70.204
3	IPA	93.824	14.255	9.218
4	1M NaOH	93.864	64.496	40.005
5	Acetone	93.904	49.330	24.009
6	H_2O	93.810	39.228	20.190
7	1 M $CaCl_2$	93.797	0.536	0.322
8	1 M NH_4OH	93.891	28.992	12.219
9	1 M Na_2CO_3	93.864	0.523	3.376
10	1 M $NaHCO_3$	93.810	0.040	1.581
11	0.1 M NaOH	93.837	57.020	34.003

Table S3
Comparison of adsorption efficiency with individual adsorbents and dual adsorbent

Time (h)	% adsorption of CR dye using various adsorbents		
	Dead biomass with wheat bran	Wheat bran	Dead biomass
1	88.286	72.04	48.64
2	90.080	74.36	51.28
3	91.124	75.28	54.35
4	92.289	76.08	56.18
5	93.534	77.52	57.43
6	94.043	78.39	58.24
7	94.471	79.66	59.56
8	94.618	80.14	60.38
9	94.618	80.22	61.15
10	94.618	80.22	61.44